Dynamics of a Bacterial Cu(I)-ATPase in a Native Lipid Environment

Henriette E. Autzen[1,2,3*], Heidi Koldsø[4], Phillip J. Stansfeld[4], Pontus Gourdon[3], Mark S. P. Sansom[4], Poul Nissen[1,2]

1 Centre for Membrane Pumps in Cells and Disease (PUMPkin), Danish National Research Foundation, Aarhus, Denmark

2 Department of Molecular Biology and Genetics, Aarhus University, Gustav Wieds vej 10C, 8000 Aarhus C, Denmark

3 Department of Biomedical Sciences, University of Copenhagen, Blegdamsvej 3, 2200 Copenhagen N, Denmark

4 Department of Biochemistry, University of Oxford, South Parks Road, Oxford OX1 3QU, United Kingdom

ABSTRACT: Lipids such as phospholipids and sterols play multiple roles in cells. Not only do they establish barriers between compartments, they also provide the matrix for assembly and function of a large variety of catalytic processes. Lipid composition is a highly regulated feature of biological membranes yet its implications on membrane proteins and their surrounding lipids is rarely approached. This is likely due to the inherent complexity of these interactions along with the difficulties associated with elucidating them. However, lipid interactions are pivotal for membrane protein function and should not be ignored. The enzyme activity of several different P-type ATPases, which constitute a large family of primary active transporters, has previously been shown to exhibit a strong dependence on phospholipids; however, distinguishing between annular and specific lipid interactions is often difficult. Our studies show for the first time that the hydrolytic activity of a bacterial Cu(I)-transporting P-type ATPase (LpCopA) is stimulated by the bacterial, anionic phospholipid cardiolipin and to some extent phosphatidylglycerol. These observations are corroborated by simulations which pinpoint lipid hotspots at the amphipathic platform helix of LpCopA. Together, the findings indicate that the stimulatory effects of LpCopA happen through specific lipid interaction sites important for protein function.

INTRODUCTION

The Cu(I)-transporting P-type ATPase, CopA, partake in the regulation of Cu(I) through active transport across membranes in a wide range of organisms. In gram-negative bacteria, CopA is part of the copper tolerance system which protects the organism from copper stress.[1] Specifically, CopA is located in the inner membrane and extrudes Cu(I) from the cytoplasm to the periplasm where the metal is either bound to chaperones or further oxidized into Cu(II).[2] Humans have two CopA proteins, ATP7A and ATP7B, which are both of critical importance for Cu(I) homeostasis, and implicated in the hereditary diseases, Menkes and Wilson's disease, respectively.[3,4]

The first published, high-resolution CopA structure was from the gram-negative bacterium Legionella pneumophila (LpCopA) (**Figure 1a**).[5] The structure is consistent with the over-all P-type ATPase domain organization with the three structurally conserved cytoplasmic domains (A, P and N, respectively) and a transmembrane domain (M-domain) which is comprised by eight α-helices. Unfortunately, the cytoplasmic, N-terminal metal binding domain (MBD), which is a unique feature of PIB-ATPases such as LpCopA, was not fully

evident in LpCopA or any of the later determined PIB-structures due to insufficient electron density; however, the crystallographic data as well as cryo electron microscopy suggest that it is located peripheral to the A-domain and is likely flexible in the determined states.[5-8] The structure of LpCopA provided valuable, new insight into the spatial arrangement of the two N-terminal α-helices, MA and MB, which are also unique to transition metal transporting P-type ATPases such as LpCopA. MB bends half-way, positioning its C-terminal part (termed MBb) in a perpendicular orientation with respect to the remaining part of the M-domain. The kink of MB is facilitated by two conserved glycine residues, a location for missense mutations in the two human CopA proteins, ATP7A and ATP7B, both of critical importance for Cu(I)-homeostasis.[5,9] Strikingly, MBb is amphipathic, a conserved nature of CopA and homologous proteins,[5] and is proposed to be located in the membrane plane at the membrane-water interface (**Figure 1b**). The functional role of the amphipathic MBb helix is not yet established; however, a dominant hypothesis is that it works as a
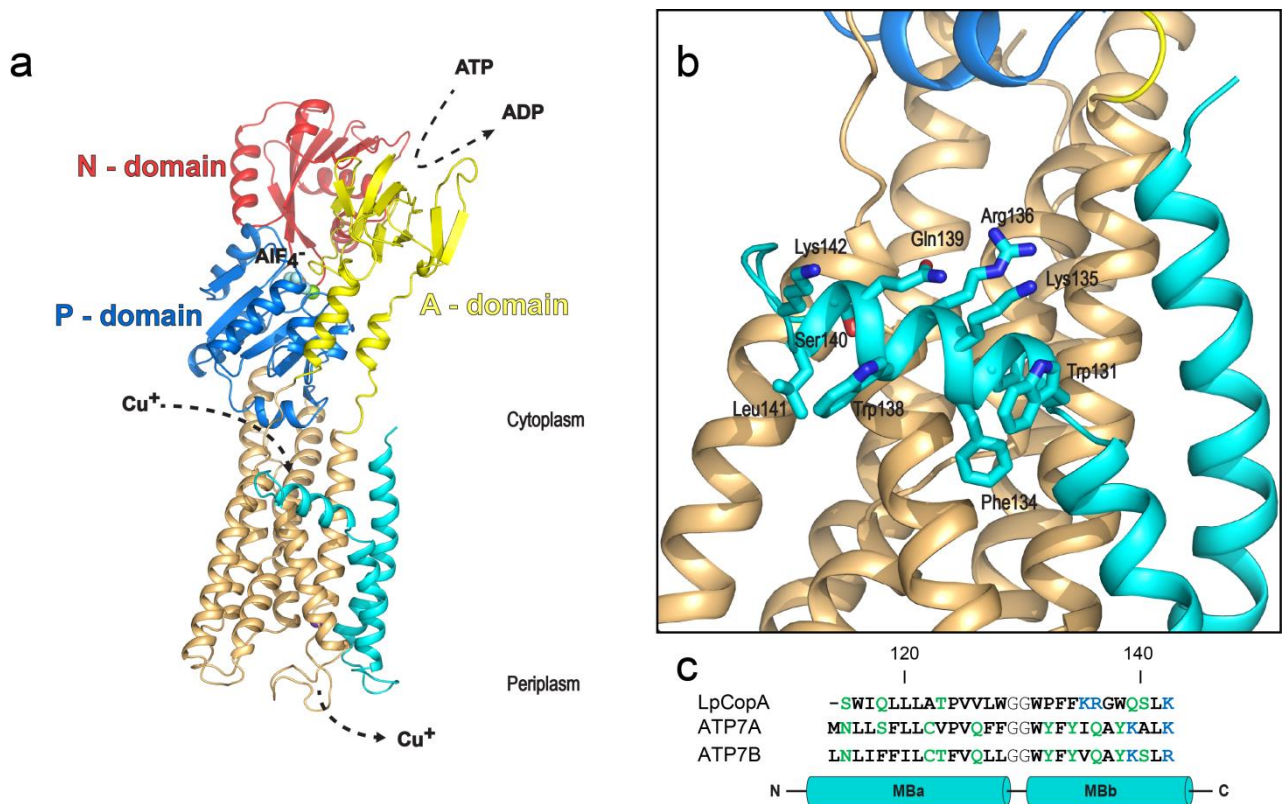
Figure 1. Primary and tertiary structures of LpCopA. (a) The crystal structure of LpCopA (PDB ID 3RFU5) showing the domain organization of LpCopA. The determined structure comprises three cytoplasmic domains and a M-domain which consists of eight α-helices. (b) Residues constituting the amphipathic MBb platform helix. (c) Multiple sequence alignment of the MB of LpCopA and the two human ATP7A (Menkes, Q04656) and ATP7B (Wilson, P35670) CopA proteins. Charged and polar residues are colored blue and green, respectively. Numbering is according to LpCopA. The alignment was produced using the CLC Genomics Workbench25 employing a Gap open and extension cost of 10 and 1, respectively.

docking site for soluble Cu(I)-chaperones which may bind through electrostatic protein-protein interactions and deliver Cu(I) directly to the transmembrane binding sites of the ATPase.[10-12] However, not all CopA proteins have a protein Cu(I)-chaperone associated with it; LpCopA is predicted to be dependent on small molecule chaperones such as glutathione or cysteine in vivo to function. As the nature of MBb proposedly positions LpCopA at the border between the cytoplasm and the membrane, electrostatic interactions with anionic lipids are likely crucial for the conformational stabilization of CopA ATPases in the membrane during transport. According to alignments of LpCopA and the human proteins, the charge and polarity of the MBb helix is distributed differently between orthologs (**Figure 1c**). This difference is likely to reflect discrepancies in how the ATPases undergo conformational changes as well as interact with the surrounding bilayer.

Most of the existing knowledge on phospholipid metabolism, function and composition in gram-negative bacteria derives from studies of the archetypal *E. coli*, but is generally believed to be transferable to most other gram-negative bacteria. The typical phospholipids in *E. coli* are phosphatidylethanolamine (PE), phosphatidylglycerol (PG) and cardiolipin (CL), accounting for most of the inner membrane (both leaflets) and the outer membrane (inner leaflet only) (**Figure 2a**). The outer leaflet of the outer membrane consists almost exclusively of lipopolysaccharides. Most distinctively, virtually all bacterial membranes contain the anionic or acidic lipids PG and CL, which in eukaryotic cells is largely confined to the mitochondrial membrane, reminiscent of its bacterial origin.[13]

Lipid compositions of bacterial membranes vary considerably over the cell life cycle and in particular with the growth temperature and the nutrition, so no generic composition can be defined; however, an estimate of the composition of the inner membrane in *E.coli* is generally reported as 70-80 % PE, 20-25 % PG, and 5-10% CL. [12,13]

By now it is well-established that lipids influence the functional properties of membrane-associated processes either through direct or indirect effects. The hydrolytic activity of P-type ATPases has previously been shown to exhibit a strong dependence on phospholipids, either on a specific head group or on the fatty acid hydrocarbon chain length or degree of saturation; examples of mammalian P-type ATPases include the Na+,K+-ATPase,[14-17] the Sarco(endo)plasmic reticulum Ca(II)-ATPase (SERCA),[18] while bacterial proteins include a Zn(II)-ATPase (ZntA) and Mg(II) ATPase (MgtA) from *E. coli*.[19,20]

Notably, the hydrolytic activity of ZntA and MgtA were recently reported as being stimulated by PG and CL, respectively.[19,20]

To address the role of MBb in LpCopA, it is crucial to understand the dynamic protein-lipid interplay which is missing from the detergent-stabilized protein structures. Thus, in this study, the protein-lipid interactions of LpCopA were investigated through *in vitro* and *in silico* characterization of the protein in a near-native lipid environment. *In vitro*, the hydrolytic activity of the purified, detergent-solubilized LpCopA in lipid-detergent micelles was largely dependent on the lipid type. Particularly, the bacterial, anionic lipid CL was identified as the strongest activating phospholipid, while the anionic 16:0-18:1 PG was also observed to stimulate the ATPase activity to some extent. Serial multiscale molecular dynamics (MD) which combines coarse-grained (CG) and atomistic (AT) simulations was used to assess the protein-lipid interactions of LpCopA in a bilayer resembling the inner bacterial membrane *in silico*. CG simulations have proven excellent for pinpointing lipid-protein interactions due to the increased lipid diffusion. Indeed, recent CG studies have successfully identified CL binding sites on the cytochrome *bc₁*[21] and cytochrome *c* oxidase,[22] and phosphatidylinositol 4,5-bisphosphate binding sites on Kir channels,[23] which each have an effect on the activity of these proteins. In the current study, the CG simulations highlight CL, and to some extent PG, as the dominant interaction partner at the MBb and other selected areas on the surface of the M-domain.

MATERIALS AND METHODS

The phospholipids 1-palmitoyl-2-oleoyl-*sn*-glycero-3-phosphocholine (POPC), 1-palmitoyl-2-oleoyl phosphatidylethanolamine (POPE), 1-palmitoyl-2-oleoyl-*sn*-glycero-3-phospho-(1'-rac-glycerol) (POPG), 1',3'-bis[1,2-dioleoyl-*sn*-glycero-3-phospho]-*sn*-glycerol (CL), 1,2-dioleoyl-*sn*-glycero-3-phosphocholine (DOPC), 1,2-dioleoyl-*sn*-glycero-3-phospho-(1'-rac-glycerol) (DOPG) and *E. coli* polar lipid extract (67 % PE, 23.2 % PG, 9.8 % CL) were purchased from Avanti Polar Lipids, Alabaster, Alabama. Octaethylene glycol monododecyl ether (C12E8) was purchased from Nikko Chemicals, Tokyo, Japan. Adenosine 5'-triphosphate disodium salt hydrate (ATP) was purchased from Sigma-Aldrich. All reagents were of highest commercial grade.

Protein Expression and Purification

Overproduction and purification of recombinant LpCopA constructs followed the well-established procedure described previously.[5] In short, the protein was overproduced in *E. coli* and cells were broken in a high-pressure homogenizer. Membranes were isolated, resuspended and solubilized with C12E8 at a final concentration of 18.6 mM. The protein was in turn purified by nickel affinity and size-exclusion chromatography in a final buffer containing 20 mM MOPS-KOH pH 6.8, 80 mM KCl, 3 mM MgCl₂, 0.28 mM C12E8, 2 mM tris(2-carboxyethyl)phosphine (TCEP) and

20 % (v/v) glycerol. Upon size-exclusion, the fractions containing LpCopA were pooled and concentrated to 10 mg/mL. Aliquots of 100 µL were flash frozen in liquid nitrogen and stored at -80 °C until their use in functional experiments.

ATPase Activity Assays

The ATPase activity of the lipid-detergent solubilized LpCopA was assessed by measuring the production of free phosphate in a modified colorimetric ATPase assay adapted from Baginski.[24] While LpCopA transports Cu(I) *in vivo* it can also transport Ag(I) as shown by us and others previously.[5,25] In our experience, LpCopA only displays significant levels of Cu(I)-activity at pH 7.0 in the presence of 200 times more L-cysteine than protein, while glutathione, BME, dithiothreitol (DTT) and TCEP are insufficient. However, in complex with each other, copper and L-cysteine has a high propensity to precipitate[26] which we also observed when performing the assays at 37 °C (data not shown). We found that while all the before mentioned thiols quenched the Ag(I)-activity of LpCopA, TCEP produced more consistent measurements of the Ag(I)-activity.

Several different lipid compositions were assessed. In general, the lipids were prepared freshly from chloroform-solubilized stocks dried in glass tubes under a nitrogen stream and incubated in a desiccator for 3 h to remove residual solvent. The dried lipids were subsequently suspended in 46.4 mM C12E8 at a final lipid concentration of 2 mg/mL until clear. The ATPase assay was performed at 37 ºC in a 50 µL reaction mixture containing 50 mM MOPS-KOH (pH 7.0), 75 mM Na₂SO₄, 5 mM KNO₃, 0.14 mg/mL of the solubilized lipid, 5.6 mM C12E8 500 µM AgNO₃, 2 mM TCEP and 10 µg LpCopA. The reactions were started by the addition of 5 mM MgSO₄-ATP (pH 7.0) and further incubated for 10 or 13 min at 37 °C which are within the linear range (**Figure S1**) The reactions were terminated with 50 µL freshly prepared development solution (141.9 mM ascorbic acid, 416.6 mM HCl, 0.08 % SDS, 4.2 µM ammonium heptamolybdate tetrahydrate) added at RT. The color development was stopped after 10 minutes by adding 75 µL stop solution (154.0 mM sodium (meta)arsenite, 77.5 mM trisodium citrate, 0.35 M ice-acetic acid) and allowed to fully develop for 20 minutes before absorption measurement at 860 nm on a PerkinElmer Victor3 plate reader. A range of different K₂HPO₄ concentrations in the appropriate reaction buffer were used for deriving standard curves. Experiments were performed in technical triplicates; however, observations were verified by biological duplicates.

Molecular Dynamics Simulations

AT-MD simulations allow exploration of the single-molecule interactions of a membrane protein with a ligand and/or its native lipid environment, as in this case a bacterial membrane. However, a major problem is how to accurately incorporate the protein in a complex bilayer with as little bias of the lipid positions in the starting structure as possible, and to obtain a well equilibrated membrane-protein system. Adopting a serial multiscale

approach, which combines CG- and AT-MD simulations, offers one of the best available routes to this.[27] An overview of the procedure utilized in this study is summarized in **Figure 2b**. In the setup, CG-MD simulations are first used to assemble a lipid bilayer around the protein as well as efficiently explore the membrane protein-lipid interactions on the μs timescale. After assembly, the system configuration from the CG simulation, in this study the final frame of the simulation, is converted into an AT representation for further refinement and detailed characterization of the captured lipid-protein interactions in an AT-MD simulation.

CG-MD simulations

All CG-MD simulations were performed using the GROMACS simulation package 4.6.3[28] employing the MARTINI 2.2 CG force field,[29,30] at a temperature of 323 K. The MARTINI model uses an approximate four-to-one AT to CG bead mapping, i.e. four heavy atoms is represented by a single bead;[29] the only exception to this aromatic groups and small molecules which are mapped with a higher resolution. Amino acids consist of a single backbone bead and up to four sidechain beads. Chemical groups are represented by four main bead types: charged, non-polar, apolar and polar, which are further divided into subtypes (18 types in v.2.0 of Martini and beyond) according to their hydrogen-bonding capabilities (donor, acceptor, both or none) and their degree of polarity. The standard water model, in which a single water bead represents four water molecules, was employed in all simulations while sodium and chloride were added to neutralize the system.

The CG protein model was built from the 3.2 Å resolution structure of LpCopA captured in metal-free $E_2 \cdot P_i$-AlF_4^- state (chain A from PDB ID 3RFU). The phosphylation mimic, AlF_4^-, present in the PDB structure was converted into a phosphate covalently bound to Asp426 due to the lack P_i parameters in MARTINI 2.2. The phosphorylation site was also occupied by Mg. The tertiary structure of LpCopA was stabilized by an elastic network[31] employing a force constant of 1000 kJ·mol⁻¹·nm⁻² with a lower and upper elastic bond cut-off to 0.5 and 0.9 nm, respectively.

CG self-assembly of the bilayer was achieved by 100 ns of MD simulation with 100 % POPC lipids and this system was in turn converted into the desired lipid mixtures (**Figure 2b**). This was necessary for obtaining identical lipid compositions of the two membrane leaflets (here referred to as symmetric). Briefly, the AT LpCopA structure was oriented with MEMEMBED [32], roughly positioning the membrane normal parallel to the z-axis and predicting the membrane-spanning segment of LpCopA for later addition of the lipids. LpCopA was then converted into a CG representation, at which point POPC lipids were added in random orientations adhering to a periodic box size with a minimum distance of 50 Å between the protein and the box wall in the x- and y-directions. The box lengths were at least 120 Å in all dimensions. Finally, the system, which comprises 631 lipids, was solubilized with water particles and

neutralized with Na⁺ and Cl⁻ ions at an ionic strength of 150 mM and simulated for 100 ns.

After 100 ns of simulation, the assembled POPC bilayer was converted into a complex, symmetric bilayer consisting of the zwitterionic lipid palmitoyl oleoyl phosphatidylethanolamine (POPE) and the anionic lipids palmitoyl oleyl phosphatidylglycerol (POPG) and CL in a molecular ratio of 70:20:10 (Error! Reference source not found.**b**) This ratio roughly corresponds to the lipid composition of *E. coli* lipid polar extract and the bacterial inner membrane.[13,33] The exchange was achieved using a locally written script, generating three unique, complex systems (A-C), which were allowed to run for 1 μs each (4 μs in "real-time") after a short minimization. The complex systems comprise 574 lipid molecules each. As reference systems systems containing only POPE were also set up. All the simulation systems are summarized in Table 1.

Prior to and in between the two MD simulations (100 ns self-assembly and 100 ns production run), the systems were energy minimized for 5000 steps of steepest decent energy minimization. The simulations were run using a 20 fs time step. Non-bonded interactions were shifted to zero using the standard cutoff schemes in MARTINI; the Lennard-Jones interactions were shifted in the range of 0.9-1.2 nm and the electrostatic interactions in the range of 0.0-1.2 nm. The neighbor list was updated every ten steps and the temperature was kept constant at 323 K. The temperature and pressure were controlled by the Berendsen coupling algorithm [34] with time constants τ_t = 1.0 ps for temperature and τ_p = 1.0 ps for pressure, respectively.

Table 1. Summary of the MD simulations.

System	Bilayer composition (molecular ratio %)	Simulation time (ns)
CG#1-A, -B, -C	POPE(70):POPG(20):CL(10)	3x 1000
CG#2-A, -B, -C	POPE (100)	3x 1000
AT-A, -B, -C	POPE(70):POPG(20):CL(10)	3x 100

AT-MD simulations

The final snapshots from CG #1A, -B and -C were converted into AT representations using the CG2AT protocol described by Stansfeld *et al.*[27] which incorporates Alchembed[35] and the systems were run for another 100 ns each. As in the CG simulations, the phosphate mimic, AlF_4^- was simulated as phosphate covalently bound to Asp426.

The AT simulations were performed using the GROMACS simulation package 4.6.3,[28] employing the united atom Gromos53a6 force field[36] at a temperature of 300 K. Before the production run of 100 ns, the systems were energy minimized for 5000 steps and subjected to a 1 ns MD simulation for equilibration. The temperature was coupled using velocity rescaling, and the Parrinello-Rahman method was used for controlling the pressure.[37]
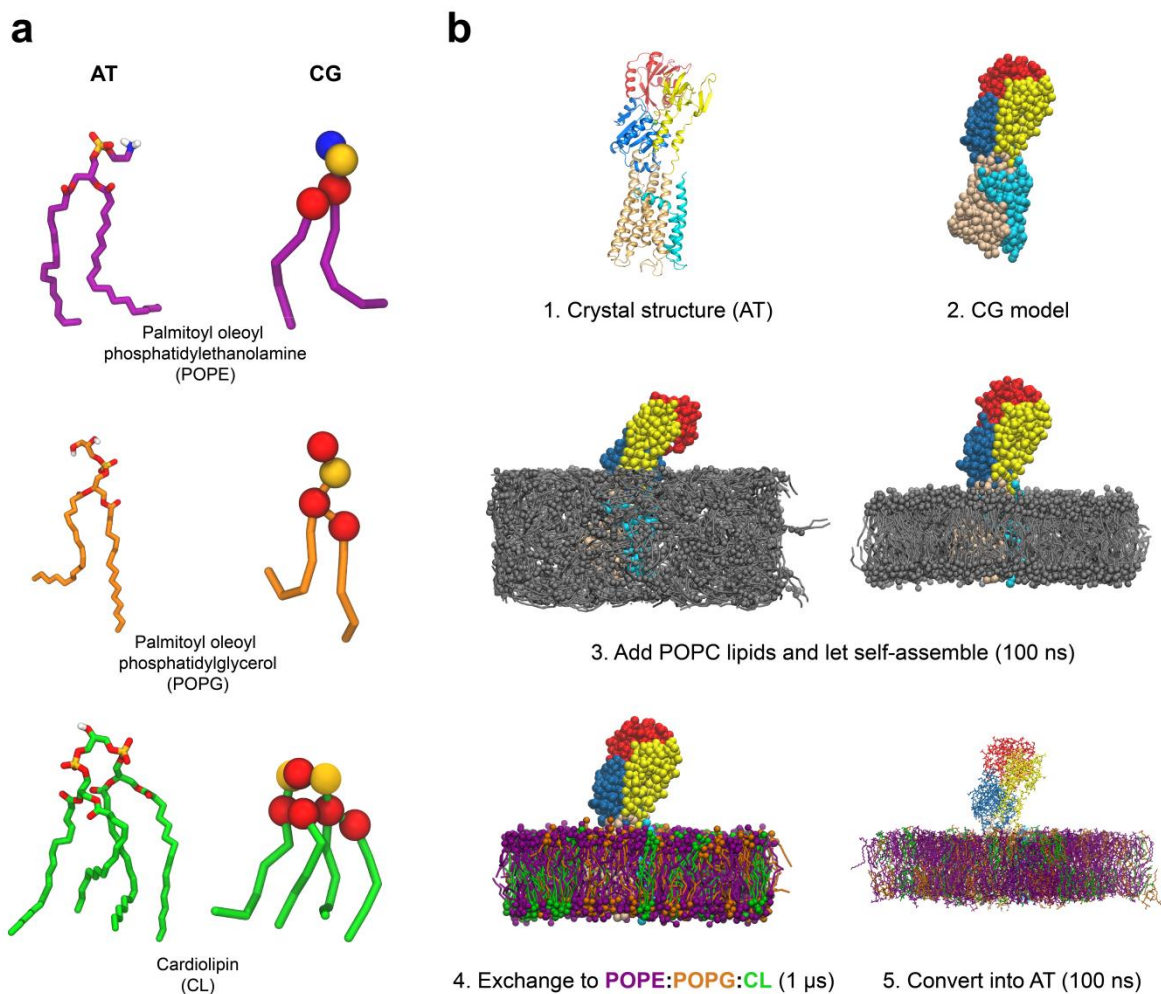
Figure 2. (a) Lipid CG and AT structures. AT lipids as they appear in the Gromos53a6 force field used in this study. The CG lipid tails are shown in sticks while head groups are shown as beads. AT lipids are shown in sticks. The fatty-acid chains of POPE, POPG and CL are colored purple, orange and green, respectively, while the head groups are colored red (ester), golden (phosphate) and blue (amine). Head group bead names and types are noted in the CG representation. (b) Overview of the MD multiscale approach starting from the AT protein crystal structure and ending with an AT system with a complex membrane. LpCopA is either represented in beads (CG) or as cartoon (AT), with MA-B in cyan, M1-6 in wheat, the A-domain in yellow, the P-domain in marine and the N-domain in red. Solvent is omitted for clarity. First the AT crystal structure of LpCopA (PDB ID 3RFU5) is converted into a CG representation (step 1 and 2). Next, POPC lipids are randomly placed around the M domain and allowed to self-assemble around LpCopA during 100 ns MD simulation (step 3). The assembled bilayer is converted into a complex, symmetric bilayer consisting of the zwitterionic POPE and the anionic POPG and CL phospholipids in a molecular ratio of 70:20:10 and simulated for 1 μs (step 4). The final snapshots from the #1A-C CG simulations were converted into an AT representation and simulated for 100 ns each (step 5).

Electrostatics was fully accounted for by applying the Particle Mesh Ewald method with periodic boundary conditions [38]. The vdW interactions were truncated at 12 Å, applying a switching function at 10 Å. The neighbor-list containing all pairs of atoms for which non-bonded interactions were calculated, included atoms within 12 Å of each other and was updated for every 10 steps. The simulations employed a time step of 2 fs, while default settings were employed for the evaluation frequency of bonded and non-bonded interactions.

Analysis of MD data

Structures were visualized using VMD and PyMol and analysis was performed using VMD and locally-written scripts. The composition of the immediate lipid environment of LpCopA, the lipid annulus, was monitored for the entire 1 μs trajectories of the three CG systems #1-A, -B and -C employing a 6 Å cutoff between protein and lipid beads as the only requirement. The mean annulus percentages were assessed by a frequency distribution using a bin width of one. The percent lipid interaction for each individual amino acid residue was

calculated by extracting the number of interactions with each type of phospholipid and comparing it to the total number of lipid interactions in the entire 1 μs trajectories. This percent interaction for each residue was in turn normalized according to the prevalence of the lipid species in the systems in order to account for the lipid ratio of 70:20:10.

RESULTS

Lipid effects *in vitro*

The lipid dependence of the *in vitro* Ag(I)-ATPase activity of LpCopA was assessed using the purified and detergent-solubilized protein relipidated with one or several combinations of lipids at saturating ATP concentrations and 500 μM $AgNO_3$ to produce maximal activity (**Figure S2a** and **S2b**). In order to limit the number of variables in elucidating whether the effect was due to the fatty acid chain or the phospholipid head group, synthetic phospholipids were primarily used for the assays. Upon relipidation with 0.14 mg/mL *E. coli* polar lipid extract, the Ag(I)-ATPase activity increased almost five-fold compared to the activity of the delipidated protein with only C12E8 added (**Figure 3a**). The predominant lipid species in *E. coli* polar lipid extract is phosphatidylethanolamine (PE, 67 %), however, relipidation with 100 % of the synthetic analog POPE was only 50 % as efficient as with *E. coli* polar lipid extract. Relipidation with POPC, another zwitterionic and solvating phospholipid had the same level of effect on the ATPase activity as POPE. On the contrary, relipidation with the synthetic phospholipid derivate DOPC, which encompasses an additional oleic acid compared to POPE and POPC, induced an activity which was on the same level as the *E. coli* polar lipid extract (**Figure 3a**). Thus, increasing the disorder or fluidity of the solvating phospholipid seems to have a marked effect on the activity of LpCopA, which fits with previous studies of the Ca²⁺-ATPase (SERCA).[39,40] However, relipidations including the anionic lipids POPG or the derivate DOPG and CL in a molecular ratio of 70:20:10, corresponding roughly to the composition of the gram-negative bacterial inner membrane, increased the Ag(I)-ATPase activity to approximately the same levels (**Figure 3a**). From this it is clear that the anionic phospholipid head groups have a significant stimulatory effect on the ATPase activity of LpCopA.

In order to identify which of the two endogenous anionic phospholipid enhances the hydrolytic activity of LpCopA the most, LpCopA was relipidated with different molecular ratios of POPE, POPG and CL varied in a systematic manner while keeping the total mass of lipid and detergent constant (**Figure 3b**). Relipidations with only POPE and POPG displayed a reduced hydrolytic activity, which increased slightly with increasing amounts of POPG, however, without reaching similar levels as with 70:20:10 POPE:POPG:CL. Meanwhile, relipidations with POPE and CL, excluding POPG, showed higher overall Ag(I)-ATPase activities and underscored that the stimulatory effect originates from CL. Relipidations with
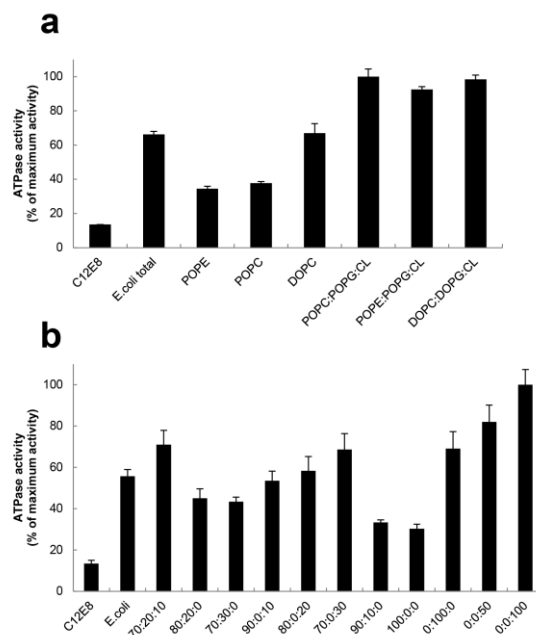

Figure 3. Activation of LpCopA by Ag(I) in lipid-detergent micelles of different compositions. The ATPase activity was measured as described in Methods. The final concentration of phospholipids and C12E8 was 0.14 mg/mL and 5.6 mM, respectively. 13 min of incubation time was used. (a) LpCopA was relipidated with *E. coli* total lipid extract, 100 % POPE, POPC, DOPC or with the anionic phospholipids PG and CL in a molecular ratio of 70:20:10. 100 % activity represents 4.8 ± 0.6 μM μg⁻¹ min⁻¹. (b) The activity was measured on the C12E8-purified LpCopA incubated with different ratios of POPE, POPG and CL as indicated. Relipidation with 100 % CL was either carried out by keeping the number of fatty acid tails the same as for POPE and POPG (0:0:50) or the same molecular ratio (0:0:100). 100 % activity corresponds to a value of 2.4 ± 0.2 μM μg⁻¹ min⁻¹).

either 100 % POPE, POPG and CL confirms these observations further, while also pointing out that the stimulatory effect of CL is concentration-dependent; *i.e.* relipidation with the same molecular ratio produced a higher hydrolytic activity than keeping the number of fatty acid tails the same as in POPE:POPG:CL 100:0:0 and 0:100:0.

Lipid effects *in silico*

In order to elucidate how the ATPase activity of LpCopA is stimulated by the anionic lipids POPG and CL *in vitro*, LpCopA was further studied *in silico* utilizing the serial multiscale MD simulation approach (ref). In this approach, which combines CG and AT MD simulations, CG MD simulations were first used to assemble a lipid bilayer around the membrane protein as well as efficiently explore the membrane protein-lipid interactions on the μs timescale. After assembly, the system configuration from the CG simulation, e.g. the final frame of the
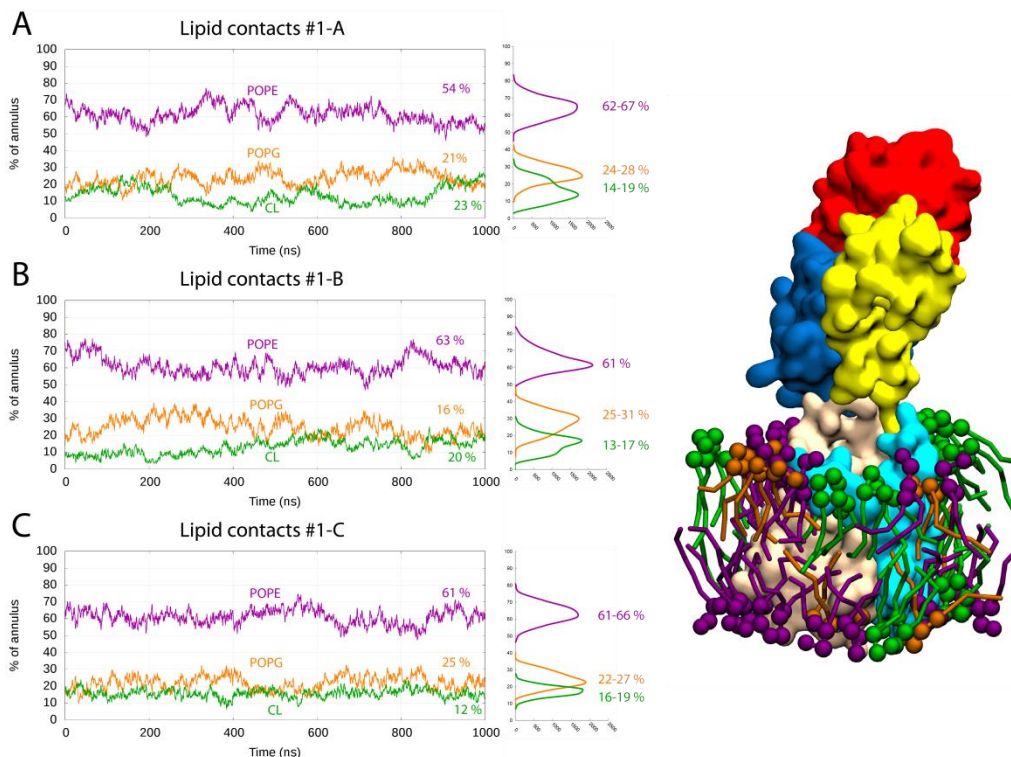
Figure 4. Lipid-protein contacts in #1 systems with bilayers consisting of 70:20:10 POPE:POPG:CL. Percentage of each lipid species in the annulus of LpCopA (employing a 6 Å cutoff between beads) relative to the total number of lipids in the annulus at the given time point in the three simulation system. The percentages in the final frame of the simulations are marked in the plots. The frequency distribution of the lipid percentages in the annulus of the three systems, calculated by using a bin width of one. The insert illustrates the final snapshot in the #1-A system of LpCopA with lipids within 6 Å of the M domain. LpCopA domains are displayed in surface representation and are colored as in previous figures.

simulation, was converted into an AT representation for further refinement and detailed characterization of the captured lipid-protein interactions in an AT MD simulation. The approach is summarized in **Figure 2b**.

LpCopA captured in the metal-free $E_2 \cdot P_i$-AlF_4^- state (chain A from PDB ID 3RFU[5]) was used to build the protein CG model. The protein was first converted to a CG representation, then positioned in a box with lipids scattered randomly around its predicted membrane spanning domain, and finally it was solvated with water and ions before it was allowed to self-assemble. CG self-assembly of the bilayer was achieved by 100 ns of MD simulation with 100 % POPC lipids, which was further converted to a complex, symmetric bilayer consisting of POPE, POPG and CL in a molecular ratio of 70:20:10 (**Figure 2b**) roughly corresponding to a bacterial inner membrane. Three such systems (#1A-C) were concomitantly produced and allowed to run for 1 µs each. The final frame from each simulation was in turn converted into an AT representation to further study the protein-lipid interactions.

The immediate lipid environment of LpCopA is enriched with POPG and CL

The composition of the immediate lipid environment of LpCopA was monitored for the entire 1 µs trajectories of the three CG systems #1-A, -B and -C (employing a 6 Å cutoff between protein and lipid beads as the only requirement). **Figure 4** provides an overview of how the annulus changes throughout the simulations; in the beginning of the simulations, the annulus has a composition of 70:20:10 of POPE, POPG and CL, which corresponds with the bilayer composition of the systems. However, during the simulations, the annulus composition changes significantly. In order to evaluate to what extent the percentages varied from the mean, the mean annulus percentages was assessed by a frequency distribution. Surprisingly, the frequency distributions show that the dominating percentage of POPE within 6 Å of LpCopA is less than 70 %, while it is more than 20 and 10 % in case of POPG and CL. These observations indicate that there is a preference of the anionic POPG and CL over the solvating lipid POPE in the annulus of LpCopA when applying a distance cutoff of 6 Å. This finding suggests that there could be specific interactions between phospholipids composing the bilayer and the transmembrane surface of LpCopA rather than random interaction corroborating with the *in vitro* observations described above. The lipid occurrence around LpCopA was assessed in further detail.
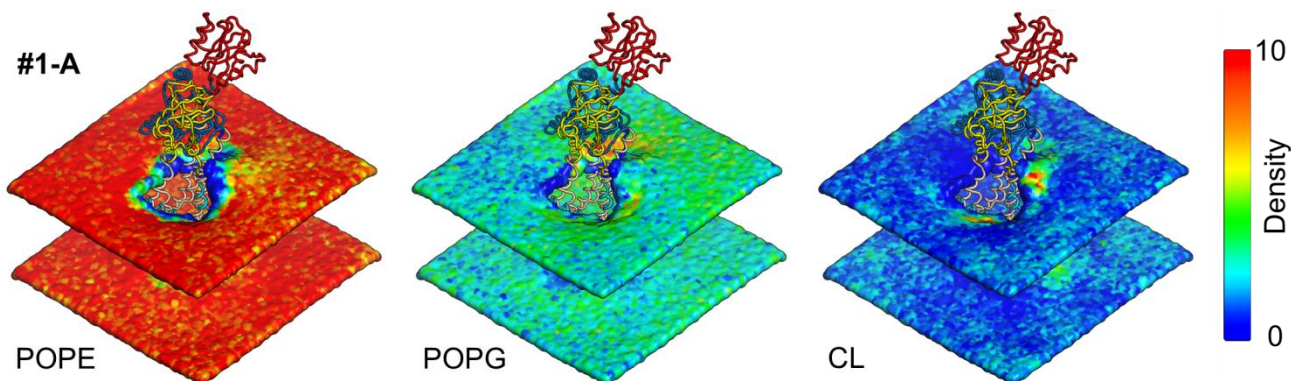
Figure 5. Averaged lipid head group densities. The average phosphate group (PO1-4) densities from the last 800 ns of the #1-A CG simulation. The densities are colored according to POPE (NH3), POPG (GLH) and CARD (PO2) head group densities respectively. Red indicates a high density (10 Å⁻²), while blue indicates a low density (0 Å⁻²). LpCopA is displayed as back bone trace and colored as in previous figures. Similar plots for all three CG systems can be seen in Supplementary Figure S3.

Lipid hotspots on the protein surface of LpCopA

In order to investigate how the lipid bilayer accommodates to LpCopA and whether there were any particularly favored areas of the three types of phospholipids in the #1 CG systems, the lipid head group densities were monitored in the last 800 ns of each trajectory. **Figure 5** shows the averaged lipid head group (PO1-4) densities from the #1-A CG system, colored according to lipid head group beads specific for one of the three lipid species (POPE [NH3]; POPG [GLH]; CL [PO2]). Plots for all three #1 CG systems can be seen in Supplementary **Figure S3**. The head group densities revealed significant local deformations near the MBb platform and the N-terminus positioned on the cytoplasmic side. The bilayer near MBb almost creates a funnel towards MBb and the ion-entry side. On the periplasmic side, the bilayer seemed to accommodate to the presumed exit pathway.

Coloring the phospholipid densities according to the lipid species head group, revealed that certain lipid hot spots might be present in the annulus of LpCopA. POPE, the dominant phospholipid of the systems, seemed less prevalent in the vicinity of LpCopA compared to the bulk of the bilayer (**Figure 5**), but occurred more at the rim of M1 and M3 than near the remaining helices. Surprisingly, POPG seemed to cluster near the C-terminal region or MBb in #1-A (**Figure 5**). In particular, CL seems to localize near MBb and the N-terminus to some extent, the two cytoplasmic areas of the membrane that also underwent significant deformations during the simulations (**Figure 5**).

The phosphate head group densities indicate that there are indeed some areas on the surface of LpCopA that could be more favored by POPG and CL over others, corroborating the observations made in the previous section. However, these results must be interpreted with caution as artifacts are likely to occur during the alignment of the protein in each frame, which could explain some of the lipid deficiency in the near vicinity of

LpCopA. Moreover, the drastic deformations observed near the N-terminus could also stem from the lack of the cytoplasmic MBD.

Single-Residue Lipid Interactions

Next, the lipid interaction for each individual amino acid residue was evaluated to estimate whether certain amino acid residues of the M-domain of LpCopA had a preference towards interacting with a certain phospholipid type. The percent lipid interaction was estimated by extracting the number of interactions that each residue of LpCopA was monitored to have with each type of phospholipid, and then calculating the percentage of this particular interaction relative to the total number of lipid interactions for each residue in the entire 1 µs trajectories. This percent interaction for each residue was in turn normalized according to the prevalence of the lipid species in the systems in order to account for the lipid ratios. The lipid interaction percentage is visualized by a gradient map on the surface of the LpCopA model in **Figure 6** for the #1-A systems and for all three systems in Supplementary **Figure S4a** and **S4b**.

It is expected that, if an interaction with a lipid is non-specific, the average interaction percentage of the residue with POPE, POPG and CL would be about 70 %, 20 % and 10 %, mirroring the ratios of the lipids used in the simulations. Some parts of the M-domain indeed display this kind of interaction with some of the lipids. However, it is clear that several residues are more likely to interact more with some of the lipid types than others. Specifically, M2, MA, MB and the MBb platform are somewhat deficit of POPE, but interacts with CL and to some extent POPG (**Figure 6**). Furthermore, the POPG interaction site near the C-terminus mentioned in the previous section is apparent from the data; however, in the #1-B and #1-C simulations this area shows a preference towards CL. It is interesting to note that POPG and CL share many of the same interaction sites, which is likely due to their head group similarity. Overall, it seems that
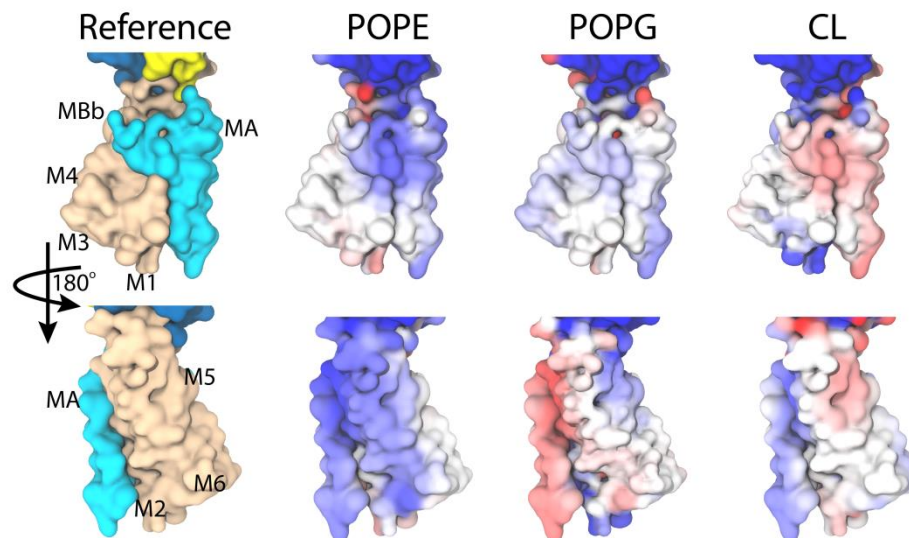
Figure 6. Lipid interaction percentage for amino acid residues in the M-domain of LpCopA in the CG simulation #1-A. The upper and lower panels show the CG M-domain of LpCopA in surface representation from two orientations, related to each other by 180º. The reference structure to the left is for orientation purposes, illustrating which transmembrane α-helices (denoted) are visible from the two orientations. The coloring values were obtained by extracting the number of lipid interactions that each amino acid residue in the M-domain was monitored to have and calculate this number as a percentage interaction relative to the total number of lipid interactions in the entire 1 µs simulation. This number was in turn normalized according to the prevalence of the lipid species in the systems in order to account for the lipid ratio of 70:20:10. Because of this normalization, the color scale is different between each of the three phospholipid types, in which a white shade denotes an interaction equal to 70 %, 20 % and 10 % for POPE, POPG and CL, respectively, while a blue shade indicates an interaction below these levels and a red shade indicates an interaction above these levels. Similar plots for all three CG systems can be seen in Supplementary Figure S4a and S4b.

several residues of the M-domain show a decreased preference towards interacting with POPE.

In order to establish which part of the phospholipids, *i.e.* the head group or acyl tail groups, is the underlying determinant of the interaction throughout the simulations, the lipid interactions were converted into a contact matrix (**Figure 7**). The matrices were made by monitoring the contacts between LpCopA and all the individual lipid bead groups within the cutoff (using 6 Å as previously) during the 1 µs of simulation and determined as the number of contacts per lipid per frame. According to the contact matrices, the head group beads were dominating interaction partners for LpCopA for all three phospholipid types in all three systems (**Figure 7** and **S5a-c**). However, in case of POPE, the majority of the acyl tail groups also constituted a significant interaction partner, while this seemed only to be the case for the terminal acyl group of POPG.

Lipid interactions on the AT scale

In order to explore the nature of the lipid-protein interactions at the amphipathic MBb helix captured in the CG simulations, the final frame from the three CG #1 systems was converted into AT representations and simulated for 100 ns each, allowing protein-lipid interactions to relax. The Cα root mean square displacement (RMSD) of the M-domain helices was measured using the starting structure as the reference (Supplementary Figure S6). According to the RMSD, the

M-domain reached equilibration within the first 10 ns to approximately 2 Å which is in the expected range for a system obtained through a CG simulation (REF).

In two of the three CG simulations, CL molecules were captured interacting with the amphipathic MBb platform in the final frame and these contacts were maintained in the AT simulations and explored further. In the AT-A simulations, two CL molecules interacted with both polar and nonpolar residues of MBb. In particular, sidechains of the basic residues, Lys135 and Lys142, pointed towards the head groups of CL (**Figure 8b** and **8d**) as opposed to Arg136 which remains completely soluble throughout the simulations, pointing towards the ion binding site. Lys135, Lys142 and to some extent Gln139 were generally observed to be half-buried and interacting with lipid phosphate head groups throughout all three AT simulations. These observations are evident from the average solvent accessible surface area (SASA) of these and the remaining MBb residues (**Figure 8c**). In general, the residues lining the lower face of MBb (Trp131, Pro132, Phe133, Phe134, Gly137, Trp138, Ser140 and Leu141) are buried in the bilayer and display a lower SASA relative to the residues on the upper face of MBb (Lys135, Arg136, Gln139 and Lys142).
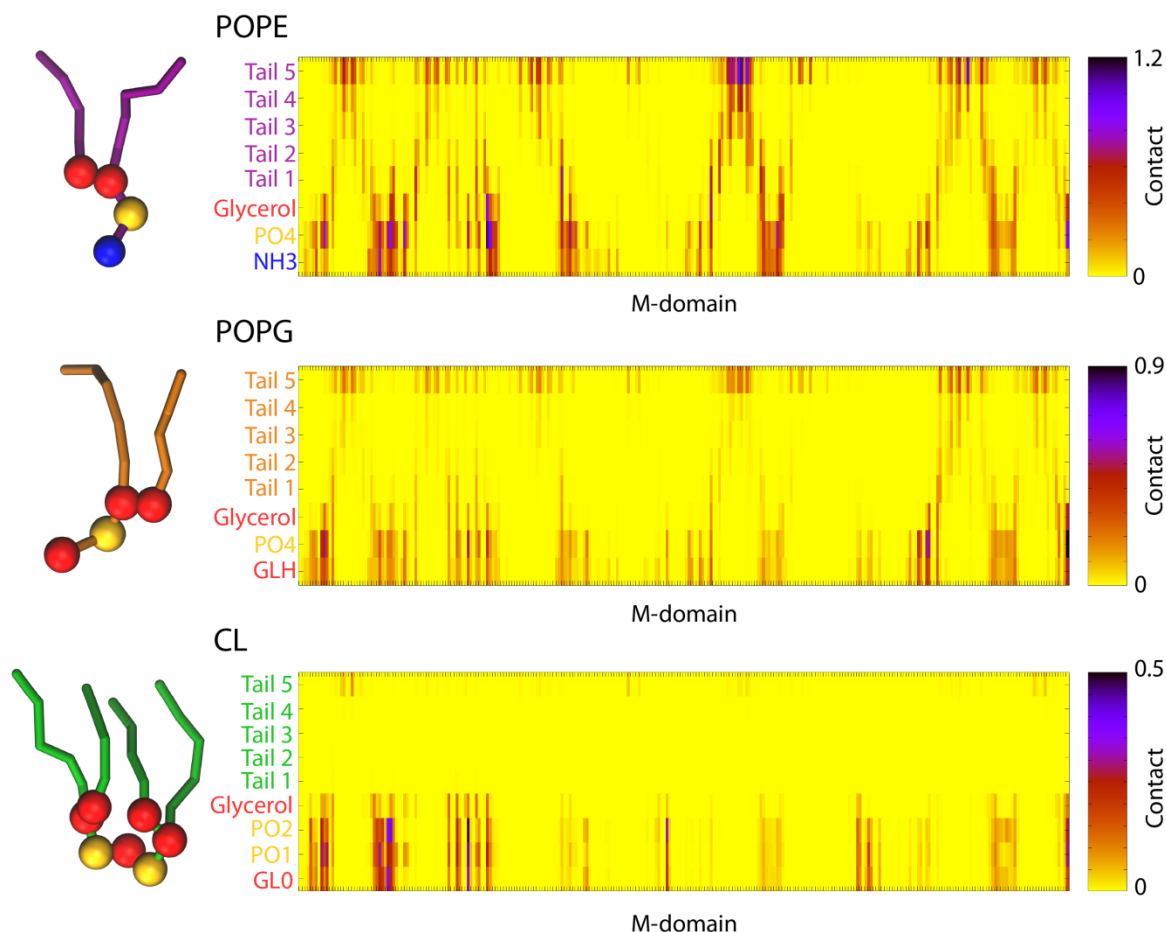
Figure 7. Contact matrix for lipid interactions with LpCopA in the #1-A systems on a yellow to blue heat map. The matrices were made by monitoring the contacts between LpCopA and the individual lipid bead groups within a 6 Å cutoff during the simulation and determined as the number of contacts per frame. The individual lipid bead groups are apparent to the left with an illustration of POPE, POPG and CL represented as previous. Similar plots for the two other #1 CG systems can be seen in Supplementary Figure S5a and S5b.

DISCUSSION

The aim of the study was to elucidate how LpCopA behaves in and depend on a native lipid environment through biochemical characterization and a serial multiscale MD approach. *In vitro*, the hydrolytic activity of the purified, detergent-solubilized LpCopA in lipid-detergent micelles was largely dependent on the lipid type used for the relipidation and particularly *E. coli* total lipid extract induced a greater hydrolytic activity than synthetic, zwitterionic lipids conventionally used for P-type ATPase activity and structural studies. The anionic lipid CL, a minor component of bacterial membranes, was identified as the strongest activating phospholipid, while the anionic POPG was observed to stimulate the ATPase activity of LpCopA to a lesser extent. While relipidations with the solvating lipids POPE and POPC produced a

more active ATPase than the detergent-stabilized, delipidated protein, they had a much weaker stimulation than CL, an observation that likely underscores the significance of anionic lipids on a bacterial membrane protein. While the increased activity is likely to be partially reflected by an enhanced fluidity of the bilayer due to a composition of mixed chain lengths, our results with the synthetic lipids clearly demonstrate that the head group of CL has an effect on the hydrolytic activity. While this is the first report of an observed stimulatory effect of CL on the hydrolytic activity of a Cu(I)/Ag(I)-transporting P-type ATPase such as LpCopA, the results corroborates with studies of two other bacterial P-type ATPases, ZntA and MgtA from *E. coli* in which the lipid dependence of the lipid-detergent micellar forms was likewise characterized.[20,21] In these studies, the hydrolytic activities of both ZntA and MgtA were increased upon the

addition of detergent solubilized *E. coli* total lipid extract. For ZntA, which is another P_{IB}-ATPase, PG was identified as the strongest activating membrane component, while CL had no effect. In contrast, CL was reported as the strongest activating lipid of MgtA while PG only increased the activity by 30 % relative to CL.

Whether the mechanism by which the anionic lipids enhance the ATPase activity of ZntA, MgtA and LpCopA in vitro is through direct or indirect effects is difficult to decipher from studies as those presented here. Thus, we decided to use serial multiscale MD simulations to probe the protein-lipid interactions of LpCopA on the single molecule level to address whether the positively charged MBb not only offers a putative interaction site for soluble MBDs and Cu(I) chaperones, but also anionic lipids. The bilayer was composed by POPE:POPG:CL in a molecular ratio of 70:20:10 roughly corresponding to the composition of a bacterial inner membrane and the *E. coli* extract as applied in the experiments *in vitro*. Assessments of the LpCopA annulus composition in the three CG1 simulations showed that the annulus is enriched with POPG and CL and highlighted CL, and to some extent POPG, as the dominant interaction partner of the M-domain of LpCopA over the solvating POPE (**Figure 4a-c**). Evaluation of the lipid interaction of each individual amino acid residue of LpCopA further indicated that there are certain 'hot-spots' on the surface of the M-domain and particularly the MBb turned out to be a region which favored interaction with CL (**Figure 5** and **Figure 6**). POPG and CL share many of the same interaction 'hot spots', which is likely due to their head group similarities. However, despite their similarity, it was clear that CL was favored over POPG and that CL interacted primarily with its head group while POPG had a higher protein interaction with its tail groups than CL (**Figure 7**).

AT MD simulations of the CL-protein interactions captured in the CG simulations show how the positively charged Lys135 and Lys142 can interact with the anionic CL and POPG phosphate head groups. In the human ATP7A and ATP7B only Lys142 is preserved, while Lys135 is instead an isovaline or a valine and MBb consequently has one less charge in the human proteins. In all three AT simulations, Arg136 and Gln139 showed the highest degree of solvation. Interestingly, Arg136 is a glutamine in the human proteins, while Gln139 is a lysine (Figure 1c), shuffling the charge distribution and hence the interactions with the local environment. While it is difficult to predict exactly what effects the difference in charge distribution and strength between the bacterial protein and the human proteins has on a functional level, it is reasonable to suggest that they have arisen in order to accommodate the differences in the membrane environments as well as the soluble interaction partners delivering the Cu(I).

In summary, our studies show for the first time that the hydrolytic activity of a bacterial Cu(I)-transporting P-type ATPase (LpCopA) is stimulated by the bacterial, anionic phospholipid CL and to some extent POPG. These observations are substantiated by simulations which pinpoint lipid hotspots at the amphipathic platform helix of LpCopA. Together, the findings presented here indicate that the stimulatory effects that the anionic lipids have on LpCopA likely happen through specific lipid interaction sites. Membranes of prokaryotic and eukaryotic cells differ considerably in lipid composition, and this aspect is particularly important when using a bacterial membrane protein as a model system for inferring knowledge on mammalian membrane proteins. Our study presented here addresses this discrepancy by elucidating how LpCopA behaves in and depend on a near-native membrane environment.

ASSOCIATED CONTENT

Supporting Information.
Figure S1-2, with details of *in vitro* activity of LpCopA.
Figure S3-S6, with details of additional analysis of CG and AT simulation data.

AUTHOR INFORMATION

Corresponding Author

*henriette.autzen@ucsf.edu
*pn@mbg.au.dk

Present Addresses

*HEA: Department of Biochemistry and Biophysics, University of California San Francisco, 600 16th St., San Francisco, CA 94158
3H.K.: D. E. Shaw Research, 120 W. 45th St., 39th Floor, New York, NY 10036

Author Contributions

The manuscript was written through contributions of all authors. All authors have given approval to the final version of the manuscript.

Notes

The authors declare no competing financial interest.

ABBREVIATIONS

LpCopA, Cu(I)-transporting P-type ATPase; MBD, metal binding domain; PE, phosphatidylethanolamine; PG, phosphatidylglycerol; CL, cardiolipin; MD, molecular dynamics; CG, coarse-grain; AT, atomistic.

REFERENCES

(Word Style "TF_References_Section"). References are placed at the end of the manuscript. Authors are responsible for the accuracy and completeness of all references. Examples of the recommended formats for the various reference types can be found at http://pubs.acs.org/page/4authors/index.html. Detailed information on reference style can be found in The ACS Style Guide, available from Oxford Press.

Insert Table of Contents artwork here

(1)   Outten, F. W.; Huffman, D. L.; Hale, J. A.; O'Halloran, T. V. *The Journal of biological chemistry* **2001**, *276*, 30670.

(2)   Singh, S. K.; Grass, G.; Rensing, C.; Montfort, W. R. *Journal of bacteriology* **2004**, *186*, 7815.

(3)   Mercer, J. F. *Trends in molecular medicine* **2001**, *7*, 64.

(4)   de Bie, P.; Muller, P.; Wijmenga, C.; Klomp, L. W. J. *J Med Genet* **2007**, *44*, 673.

(5)   Gourdon, P.; Liu, X. Y.; Skjorringe, T.; Morth, J. P.; Moller, L. B.; Pedersen, B. P.; Nissen, P. *Nature* **2011**, *475*, 59.

(6)   Andersson, M.; Mattle, D.; Sitsel, O.; Klymchuk, T.; Nielsen, A. M.; Moller, L. B.; White, S. H.; Nissen, P.; Gourdon, P. *Nature structural & molecular biology* **2014**, *21*, 43.

(7)   Wang, K.; Sitsel, O.; Meloni, G.; Autzen, H. E.; Andersson, M.; Klymchuk, T.; Nielsen, A. M.; Rees, D. C.; Nissen, P.; Gourdon, P. *Nature* **2014**.

(8)   Wu, C. C.; Rice, W. J.; Stokes, D. L. *Structure* **2008**, *16*, 976.

(9)   Gourdon, P.; Sitsel, O.; Karlsen, J. L.; Moller, L. B.; Nissen, P. *Biol Chem* **2012**, *393*, 205.

(10)   Mandal, A. K.; Arguello, J. M. *Biochemistry* **2003**, *42*, 11040.

(11)   Gonzalez-Guerrero, M.; Arguello, J. M. *Proceedings of the National Academy of Sciences of the United States of America* **2008**, *105*, 5992.

(12)   Gonzalez-Guerrero, M.; Hong, D.; Arguello, J. M. *The Journal of biological chemistry* **2009**, *284*, 20804.

(13)   Cronan, J. E. *Annual review of microbiology* **2003**, *57*, 203.

(14)   Ottolenghi, P. *European journal of biochemistry / FEBS* **1979**, *99*, 113.

(15)   Johannsson, A.; Smith, G. A.; Metcalfe, J. C. *Biochim Biophys Acta* **1981**, *641*, 416.

(16)   Shinoda, T.; Ogawa, H.; Cornelius, F.; Toyoshima, C. *Nature* **2009**, *459*, 446.

(17)   Habeck, M.; Haviv, H.; Katz, A.; Kapri-Pardes, E.; Ayciriex, S.; Shevchenko, A.; Ogawa, H.; Toyoshima, C.; Karlish, S. J. *The Journal of biological chemistry* **2015**, *290*, 4829.

(18)   Johannsson, A.; Keightley, C. A.; Smith, G. A.; Richards, C. D.; Hesketh, T. R.; Metcalfe, J. C. *The Journal of biological chemistry* **1981**, *256*, 1643.

(19)   Zimmer, J.; Doyle, D. A. *Biochim Biophys Acta* **2006**, *1758*, 645.

(20)   Subramani, S.; Perdreau-Dahl, H.; Morth, J. P. *eLife* **2016**, *5*.

(21)   Arnarez, C.; Mazat, J. P.; Elezgaray, J.; Marrink, S. J.; Periole, X. *Journal of the American Chemical Society* **2013**, *135*, 3112.

(22)   Arnarez, C.; Marrink, S. J.; Periole, X. *Scientific reports* **2013**, *3*, 1263.

(23)   Stansfeld, P. J.; Hopkinson, R.; Ashcroft, F. M.; Sansom, M. S. *Biochemistry* **2009**, *48*, 10926.

(24)   Baginski, E. S.; Foa, P. P.; Zak, B. *Clinical chemistry* **1967**, *13*, 326.

(25)   Yang, Y.; Mandal, A. K.; Bredeston, L. M.; Gonzalez-Flecha, F. L.; Arguello, J. M. *Biochim Biophys Acta* **2007**, *1768*, 495.

(26)   Rigo, A.; Corazza, A.; di Paolo, M. L.; Rossetto, M.; Ugolini, R.; Scarpa, M. *Journal of inorganic biochemistry* **2004**, *98*, 1495.

(27)   Stansfeld, P. J.; Goose, J. E.; Caffrey, M.; Carpenter, E. P.; Parker, J. L.; Newstead, S.; Sansom, M. S. *Structure* **2015**, *23*, 1350.

(28)   Hess, B.; Kutzner, C.; van der Spoel, D.; Lindahl, E. *Journal of Chemical Theory and Computation* **2008**, *4*, 435.

(29)   Marrink, S. J.; Risselada, H. J.; Yefimov, S.; Tieleman, D. P.; de Vries, A. H. *The journal of physical chemistry. B* **2007**, *111*, 7812.

(30)   Monticelli, L.; Kandasamy, S. K.; Periole, X.; Larson, R. G.; Tieleman, D. P.; Marrink, S.-J. *Journal of Chemical Theory and Computation* **2008**, *4*, 819.

(31)   Periole, X.; Cavalli, M.; Marrink, S. J.; Ceruso, M. A. *J Chem Theory Comput* **2009**, *5*, 2531.

(32)   Nugent, T.; Jones, D. T. *BMC bioinformatics* **2013**, *14*, 276.

(33)   Dowhan, W. *Annual review of biochemistry* **1997**, *66*, 199.

(34)   Berendsen, H. J. C.; Postma, J. P. M.; Vangunsteren, W. F.; Dinola, A.; Haak, J. R. *Journal of Chemical Physics* **1984**, *81*, 3684.

(35)   Jefferys, E.; Sands, Z. A.; Shi, J.; Sansom, M. S.; Fowler, P. W. *J Chem Theory Comput* **2015**, *11*, 2743.

(36)   Oostenbrink, C.; Villa, A.; Mark, A. E.; van Gunsteren, W. F. *Journal of computational chemistry* **2004**, *25*, 1656.

(37)   Parrinello, M.; Rahman, A. *J Appl Phys* **1981**, *52*, 7182.

(38)   Essmann, U.; Perera, L.; Berkowitz, M. L.; Darden, T.; Lee, H.; Pedersen, L. G. *Journal of Chemical Physics* **1995**, *103*, 8577.

(39)   Moore, B. M.; Lentz, B. R.; Meissner, G. *Biochemistry* **1978**, *17*, 5248.

(40)   Li, Y.; Ge, M.; Ciani, L.; Kuriakose, G.; Westover, E. J.; Dura, M.; Covey, D. F.; Freed, J. H.; Maxfield, F. R.; Lytton, J.; Tabas, I. *The Journal of biological chemistry* **2004**, *279*, 37030.